LANGMUIR

pubs.acs.org/Langmuir Article

SAMs on Gold Derived from Adsorbates Having Phenyl and Cyclohexyl Tail Groups Mixed with Their Phase-Incompatible Fluorinated Analogues

Tianlang Yu, Maria D. Marquez, and T. Randall Lee*

Cite This: *Langmuir* 2022, 38, 13488−13496 Read Online

ACCESS | Metrics & More | Article Recommendations | Supporting Information

ABSTRACT: This article investigates two types of mixed self-assembled monolayers (SAMs) derived from adsorbates having cyclohexyl and phenyl tail groups mixed with their perfluorinated analogues. The mixed SAMs were characterized using ellipsometry, X-ray photoelectron spectroscopy (XPS), polarization−modulation infrared reflection absorption spectroscopy, and contact angle measurements. The XPS results show preferential adsorption of the nonfluorinated adsorbate in the perfluorocyclohexyl-terminated/cyclohexyl-terminated pair due to the steric bulk of the tail groups. On the other hand, mixed surfaces with a precisely controlled surface composition were achieved with the phenyl-terminated/perfluorophenyl-terminated mixed SAMs, exhibiting a linear relationship between the mole fraction on the surface and the mole fraction in solution. The results suggest that the relative solubility, steric bulk of the tail group moiety, and the interaction between two different adsorbates are the key factors driving the phase phenomena observed in the SAMs. More importantly, this study suggests that the interfacial properties can be controlled with a minimal loss of packing densities with the phenyl-terminated/perfluorophenyl-terminated mixed SAMs.

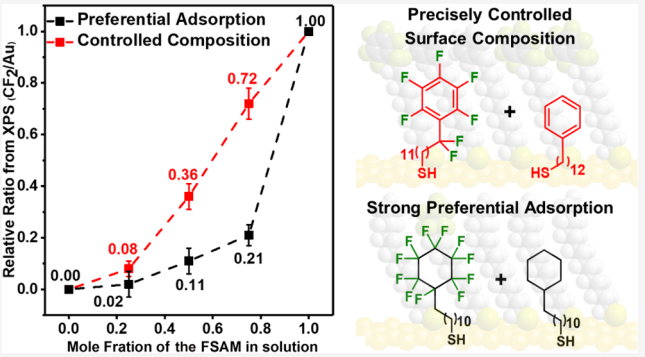

INTRODUCTION

Incorporating fluorine atoms into the molecular structure of an adsorbate renders this class of molecules excellent candidates for nanocoatings, specifically in the form of fluorinated self-assembled monolayers (FSAMs), due to their highly hydrophobic and oleophobic nature.[1,2] After decades of development, SAMs have been widely employed for surface modification in various industrial fields, such as anti-corrosion in GaAs electronic devices,[3−5] anti-fouling in biosensors,[6,7] and anti-adhesion in microelectromechanical systems.[8−10] Modification of surfaces with SAMs, such as those derived from alkanethiols, with differing chemical species (i.e., a fully hydrocarbon alkanethiol and a fluorinated alkanethiol), have attracted the attention of scientists and engineers in order to tune interfacial properties. However, due to the phase incompatibility of fluorinated and non-fluorinated adsorbates, discrepancies between the composition of the SAMs and deposition solutions are often seen.[11] Moreover, there are three major challenges that have been encountered in attempts to generate mixed, phase-incompatible SAMs: (1) preferential adsorption of one type of adsorbate over the other; (2) phase separation on the surface (i.e., the formation of molecular domains formed on the nanometer scale); and (3) changes to the composition of the surface over time due to adsorbate exchange.[12−15] For example, a previous study of mixed SAMs on Au(111) derived from the mixture of hexadecane-1-thiol and heptadecafluorohexadecane-1-thiol saw preferential adsorption of the fluorinated adsorbate due to its poor solubility and hydrophobic nature, facilitating its transition from the solution phase onto the gold surface.[16−18]

The previous literature has extensively examined the effect of combining incompatible functional groups, such as the mixed surface of methyl and hydroxymethyl groups,[12] methyl and amino groups,[19] and methyl and oligo(ethylene glycol) groups.[20] However, the number of studies exploring the effect of bulky functional groups is limited,[21−23] especially for fluorinated groups.[24−27] To study the effect of bulky perfluorinated tail groups in mixed phase-incompatible SAMs, we investigated mixed SAMs generated from two classes of adsorbates on Au(111) bearing either a cyclohexyl or phenyl tail group of the form $C_6H_{11}(CH_2)_{11}SH$ (**HCyH11SH**) and $C_6H_5(CH_2)_{12}SH$ (**PhH12SH**), respectively. The adsorbates were mixed with their perfluorinated analogues,

Received: July 26, 2022
Revised: October 10, 2022
Published: October 26, 2022

https://doi.org/10.1021/acs.langmuir.2c01991
Langmuir 2022, 38, 13488−13496

$C_6F_{11}(CH_2)_{11}SH$ (**FCyH11SH**) and $C_6F_5CF_2(CH_2)_{11}SH$ (**FPhFH11SH**), respectively, to generate the mixed surfaces on gold; the molecular structures of the adsorbates are shown in Figure 1. The adsorbates terminated with an aromatic

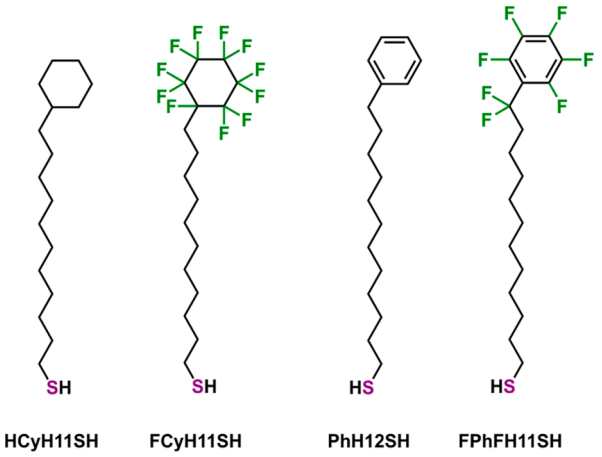

Figure 1. Molecular structures of the adsorbates used to generate mixed SAMs on gold.

moiety were included in this study in order to offer insights into the structure−property relationship of mixed SAMs with different perfluorinated tail groups. All of the adsorbates in this study have bulky tail groups compared to simple alkyl and fluoroalkyl chains, but the phenyl and perfluorophenyl tail groups are less sterically bulky than the cyclohexane and perfluorocyclohexane rings because of the planar structure of the phenyl ring. Furthermore, π-interactions between phenyl rings, as well as π-interactions between phenyl and perfluorophenyl rings, might reduce the phase separation of our mixed SAMs.[28−30]

The two series of mixed monolayers were characterized using ellipsometry, X-ray photoelectron spectroscopy (XPS), polarization−modulation infrared reflection−absorption spectroscopy (PM-IRRAS), and contact angle measurements.

EXPERIMENTAL PROCEDURES

Materials and chemicals used, details of the synthetic procedures, spectroscopic characterization data for the **FPhFH11SH** adsorbate (^{1}H, ^{19}F, and ^{13}C NMR spectra; see Figures S1−S3), instrumental methods used, and optical images of contact angles are described in the Supporting Information.

RESULTS AND DISCUSSION

The nomenclature of the mixed SAMs is defined according to the mole fraction of the fluorinated adsorbate in solution. For example, sample **FCyH11SH** (0.00) represents a SAM composed of 100% **HCyH11SH**, while **FPhFH11SH** (0.00) represents a SAM composed of 100% **PhH12SH**. A detailed overview of the composition of the SAMs are given in Table 1.

Ellipsometric Thickness Measurements. After the mixed SAMs were deposited on Au(111) for 48 h, the average thicknesses of the thin films were measured by ellipsometry. Table 2 lists the average ellipsometric thickness of the mixed SAMs on Au(111). Apparent from the data, the single-component SAMs generated from the **FCyH11SH** adsorbates show lower thicknesses than their hydrocarbon analogues; 12 Å for **FCyH11SH** (1.00) SAM versus 14 Å for **FCyH11SH** (0.00) (e.g., **HCyH11SH**), while **FPhFH11SH** (1.00) and

Table 1. Adsorbate Mole Fraction in Solution Used to Generate the Mixed SAMs

mole fraction of fluorinated adsorbate in solution	sample			
	FCyH11SH	**HCyH11SH**	**FPhFH11SH**	**PhH12SH**
0.00	0.00	1.00	0.00	1.00
0.25	0.25	0.75	0.25	0.75
0.50	0.50	0.50	0.50	0.50
0.75	0.75	0.25	0.75	0.25
1.00	1.00	0.00	1.00	0.00

Table 2. Ellipsometric Thicknesses of the Investigated Mixed SAMs

sample	thickness (Å)	sample	thickness (Å)
FCyH11SH (0.00)	14 ± 1	**FPhFH11SH** (0.00)	18 ± 1
FCyH11SH (0.25)	14 ± 1	**FPhFH11SH** (0.25)	18 ± 1
FCyH11SH (0.50)	14 ± 1	**FPhFH11SH** (0.50)	18 ± 1
FCyH11SH (0.75)	14 ± 1	**FPhFH11SH** (0.75)	17 ± 1
FCyH11SH (1.00)	12 ± 1	**FPhFH11SH** (1.00)	17 ± 1

FPhFH11SH (0.00) (e.g., **PhH12SH**) exhibited the same thickness within the measurement error (17 Å vs 18 Å). The thinner thicknesses of the **FCyH11SH** SAMs were attributed to the lower packing densities due to the larger van der Waals (vdW) radius of the fluorine atoms (1.47 Å) than that of hydrogen atoms (1.20 Å)[31] in addition to the sterically bulkier perfluorinated cyclohexyl tail group than the hydrocarbon tail group. Moreover, impacted by the bulkier tail groups of cyclohexane than the planar phenyl ring, the **HCyH11SH**/**FCyH11SH** mixed SAMs show lower thickness than the **PhH12SH**/**FPhFH11SH** mixed SAMs.

In the mixed SAMs, introduction of the fluorinated adsorbate into the deposition solution led to a decrease in the film thickness. However, based on the film thickness data alone, it is difficult to determine the phase behavior on the surface. Further insights into the composition of the films are discussed in detail in the Characterization of the Mixed SAMs by XPS section.

Characterization of the Mixed SAMs by XPS. In the analysis of organic thin films, XPS is a commonly used technique for determining the surface composition and the relative packing densities of thiol-based SAMs.[32−34] Figure 2 shows the XPS spectra of the S 2p, C 1s, and F 1s binding energy regions of the **HCyH11SH**/**FCyH11SH** mixed SAMs. The S 2p spectra gives insights into the chemical nature of the sulfur species on the surface. Bound thiolates exhibit a doublet attributed to the S $2p_{3/2}$ photoelectron at 163.0 eV and the S $2p_{3/2}$ photoelectron at 162.0 eV in a 1:2 ratio for the $2p_{1/2}$ to $2p_{3/2}$ photoelectrons, which appeared for all the SAMs in the study.[35,36] Moreover, the absence of peaks at ∼164 or ∼166 eV suggests no unbound thiol or highly oxidized sulfur species, respectively, in all the investigated SAMs.[35] For the **HCyH11SH**/**FCyH11SH** mixed SAM series, the S 2p spectra exhibits the characteristic doublet representative of a bound thiolate at ∼163.0 and ∼162.0 eV in every sample, suggesting that both alkanethiols chemically bind to the Au(111) surface.

In Figure 2a, the C 1s spectra of the **HCyH11SH** SAMs show only one peak at 284.7 eV, which indicates that the carbons of the cyclohexyl ring, the tertiary carbon, and the carbons of the alkyl chain have a similar binding energy. The C

https://doi.org/10.1021/acs.langmuir.2c01991
Langmuir 2022, 38, 13488−13496

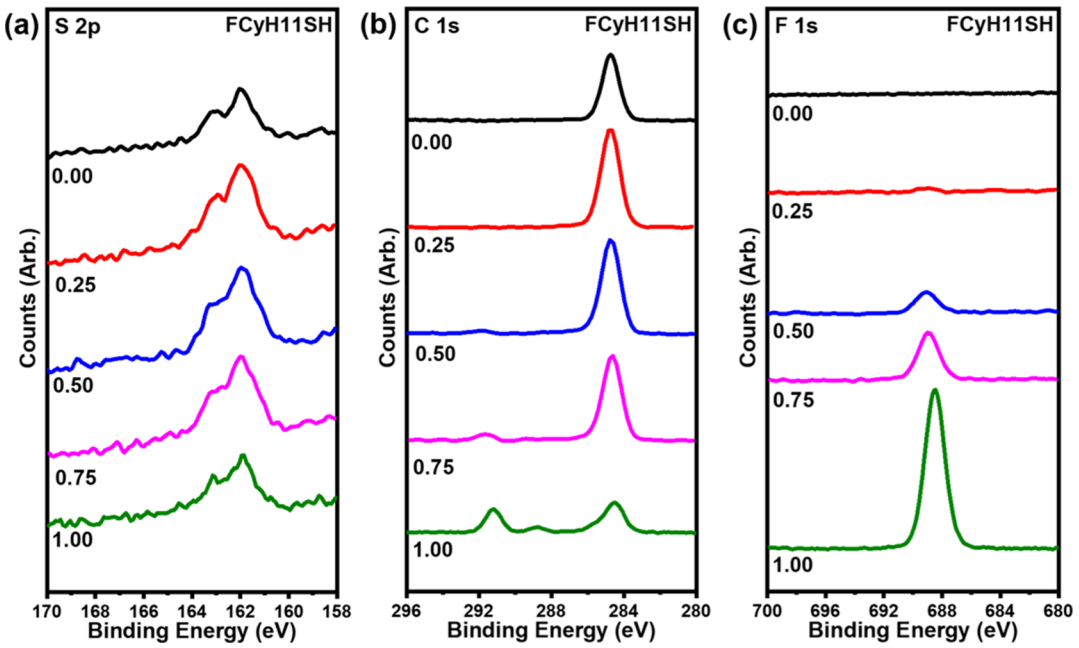

Figure 2. XPS spectra of the (a) S 2p, (b) C 1s, and (c) F 1s binding regions of the **HCyH11SH/FCyH11SH** mixed SAMs.

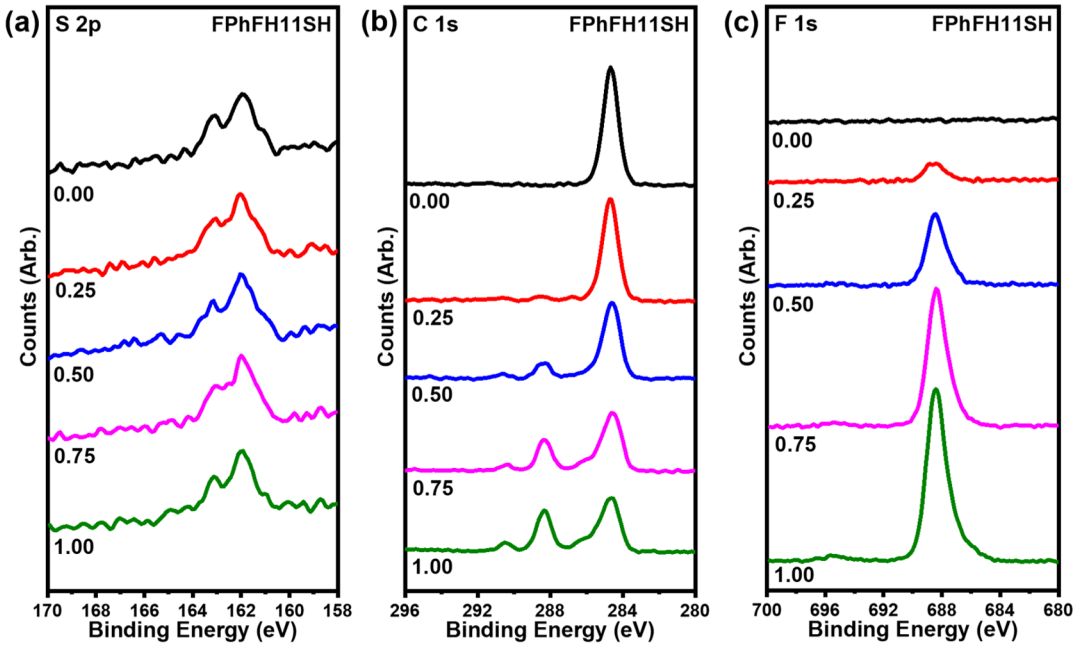

Figure 3. XPS spectra of the (a) S 2p, (b) C 1s, and (c) F 1s binding regions of the **PhH12SH/FPhFH11SH** mixed SAMs.

1s spectra of the **FCyH11SH** (1.00) SAM, shown in Figure 2b, exhibits two large peaks at 291.1 and 284.5 eV and a smaller peak at ∼288.6 eV, which are attributed to the CF_2 of the perfluorinated cyclohexane ring, CH_2 of the hydrocarbon chain, and CF connected to the alkyl chain, respectively.[2] The fluorine atoms in the perfluorocyclohexane-terminated adsorbate produced a peak in the F 1s region at 688.4 eV, as shown in Figure 2c. Apparent in the spectra, a gradual increase in the intensity of the peak is observed in the samples as the concentration of the fluorinated adsorbate increases in the deposition solution. We note also that the S 2p spectra of the **PhH12SH/FPhFH11SH** mixed SAMs in Figure 3a exhibit a characteristic doublet attributed to bound thiolate at ∼162.0 and ∼163.0 eV. For the **PhH12SH** SAM [e.g., **FPhFH11SH** (0.00)], a single peak at 284.7 eV in the C 1s spectrum was observed, as shown in Figure 3b. On the other hand, the C 1s spectrum of the **FPhFH11SH** SAM [e.g., **FPhFH11SH** (1.00)] exhibited three peaks at 290.5, 288.3, and 284.6 eV, which were attributed to electrons arising from CF_2, CF of the perfluorophenyl ring, and CH_2 of the hydrocarbon chain, respectively. Similar to that of the **FCyH11SH** SAM, the F 1s region shown in Figure 3c shows a peak at 688.4 eV, which gradually increases as the concentration of the fluorinated adsorbate increases in the deposition solution.

In addition, the relative packing density was calculated by monitoring the integrated intensity of the S 2p and Au 4f signals, specifically the S/Au ratios.[37] In our analysis, an octadecanethiol (ODT) SAM on Au was used as the reference,

https://doi.org/10.1021/acs.langmuir.2c01991
Langmuir 2022, 38, 13488−13496

in which all binding sites on the Au surface are occupied, and the packing density is 100%. Moreover, it is important to note that the electron attenuation lengths of hydrocarbons and fluorocarbons are indistinguishable, and the packing densities of the investigated thin films on Au can be calculated in the same manner.[38] Table 3 shows the relative packing densities of

Table 3. Relative Packing Densities (%)[a] of the Mixed SAMs as Determined by XPS

mole fraction of the FSAM in solution	FCyH11SH	FPhFH11SH
0.00	74 ± 5	88 ± 5
0.25	72 ± 5	83 ± 5
0.50	71 ± 5	87 ± 6
0.75	71 ± 5	88 ± 6
1.00	66 ± 5	82 ± 6

[a]To compare the relative packing densities, the S/Au ratios of the investigated SAMs were compared to that of the reference ODT SAM.

the investigated mixed SAMs. Overall, the packing densities of the mixed SAMs decreased as the mole fraction of the fluorinated adsorbate was increased in solution for both types of SAMs. The **PhH12SH/FPhFH11SH** mixed SAMs show higher packing densities than the **HCyH11SH/FCyH11SH** mixed SAMs, likely due to the different size of the chain termini. Additionally, Lee and co-workers introduced in 2016 bidentate adsorbates that exploit the "chelate effect" to generate homogeneously mixed monolayers on Au(111).[16] However, impacted by the large footprint of the bidentate head group, the packing densities (i.e., the number of molecules per unit area) of the bidentate SAMs suffer a 40% reduction compared to that of their monodentate analogues.[28] In our case, by using monodentate adsorbates instead of bidentate, the relative packing of all the investigated mixed SAMs remain 66% and above. Especially for the **PhH12SH/FPhFH11SH** mixed SAMs in different ratios, all films reach 82% and above in packing density, which is consistent with well-packed films in which the large tail groups diminish the packing densities relative to SAMs derived from normal alkanethiols.

Furthermore, the spectra in Figures 2 and 3 exhibit shifts in the peak position of the F 1s photoelectrons and the C 1s electrons originating from the carbon backbone that are dependent on the concentration of the fluorinated adsorbate in the deposition solution. Table 4 summarizes the peak positions

Table 4. C 1s Binding Energies (eV) of the CH_2 Groups in the Two Series of Mixed SAMs

mole fraction of the FSAM in solution	FCyH11SH	FPhFH11SH
0.00	284.7	284.7
0.25	284.7	284.7
0.50	284.6	284.7
0.75	284.6	284.6
1.00	284.5	284.6

for the aforementioned C 1s electrons, while Table 5 lists the binding energies of the F 1s photoelectrons. The shifts in the C 1s spectra correspond to the decreasing chain packing densities of the films and are observed in both the **HCyH11SH/FCyH11SH** and **PhH12SH/FPhFH11SH** mixed SAM systems. This phenomenon has been observed in the XPS spectra of SAMs derived from *n*-alkanethiols as well as partially

Table 5. F 1s Binding Energies (eV) of the CH_2 Groups in the Two Series of Mixed SAMs

mole fraction of the FSAM in solution	FCyH11SH	FPhFH11SH
0.00		
0.25	~689.3	688.6
0.50	689.2	688.4
0.75	689.0	688.4
1.00	688.4	688.4

fluorinated alkanethiols, where the positive charge generated from X-ray irradiation is easily discharged in SAMs having diminished chain packing densities; the energy required to emit photoelectrons from loosely packed SAMs (i.e., low C 1s binding energy) is less than that from densely packed SAMs (i.e., high C 1s binding energy).[32,39] More importantly, the results highlighted in Tables 4 and 5 are consistent with the relative packing density calculated from the integrated intensity of the S 2p and Au 4f signals. We observed a similar trend in the F 1s peak positions, where in the **HCyH11SH/FCyH11SH** system, the binding energies decease from ~689.3 to 688.4 eV as the concentration of the fluorinated adsorbate increases in the deposition solution; similarly, in the **PhH12SH/FPhFH11SH** SAMs, the peak position decreases from 688.6 to 688.4 eV when the concentration of **FPhFH11SH** is ≥0.50.

Quantitative Analysis of the Mixed SAMs: Surface Composition. To determine the composition of the mixed SAMs, the fluorocarbon (specifically, CF_2) and fluorine signals were used to evaluate the relative concentration of the fluorinated adsorbate on the surface of the mixed SAMs. For the **HCyH11SH/FCyH11SH** series, the relative ratios of the integrated intensity (peak area) of CF_2/Au and F/Au were calculated and are shown in Figure 4. It should be noted that the **FCyH11SH** (1.00) SAM was used as a reference and set to a ratio of 1.00. Figure 4a shows that the CF_2/Au ratios from **FCyH11SH** (0.25), **FCyH11SH** (0.50), and **FCyH11SH** (0.75) only reached 0.02, 0.11, and 0.21, respectively. Similarly, the F/Au ratios, shown in Figure 4b, for **FCyH11SH** (0.25), **FCyH11SH** (0.50), and **FCyH11SH** (0.75) were 0.02, 0.11, and 0.21, respectively. The results indicate that these films were mainly composed of **HCyH11SH** adsorbates with a small amount of **FCyH11SH**. Interestingly, our data show significant preferential adsorption of the hydrocarbon adsorbate over the fluorinated analogue, a trend opposite to that observed in the hexadecane-1-thiol and heptadecafluorohexadecane-1-thiol system (vide supra).[16−18] The observed preferential adsorption of the hydrocarbon adsorbate over that of the fluorinated component in the **HCyH11SH/FCyH11SH** series suggests that there are other factors at play than the solubility of the adsorbate alone. A previous study from Yu et al. stated that both **HCyH11SH** and **FCyH11SH** SAMs exhibit low packing densities compared to normal alkanethiols due to their bulky termini.[9] Additionally, the SAM generated from **FCyH11SH** was found to be more rigid and less densely packed than its hydrocarbon analogue, impacted by the larger vdW volume of the fluorine atoms.[2,26] Therefore, despite the difference in solubility, the large and rigid chain termini of the **FCyH11SH** adsorbate likely hinder its adsorption onto the surface.

A similar approach was taken in the analysis of **PhH12SH/FPhFH11SH**, where the relative ratios of CF/Au and F/Au from the XPS data were used to calculate the surface

https://doi.org/10.1021/acs.langmuir.2c01991
Langmuir 2022, 38, 13488−13496

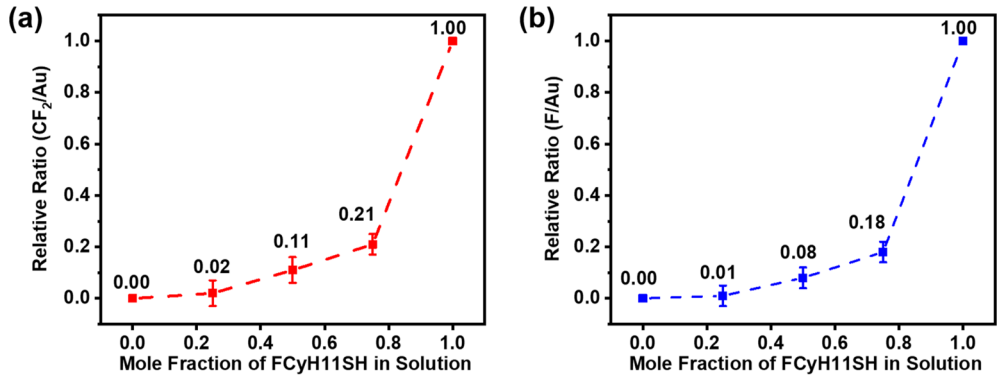

Figure 4. (a) CF_2/Au ratio and (b) F/Au ratio of the **HCyH11SH/FCyH11SH** mixed SAMs.

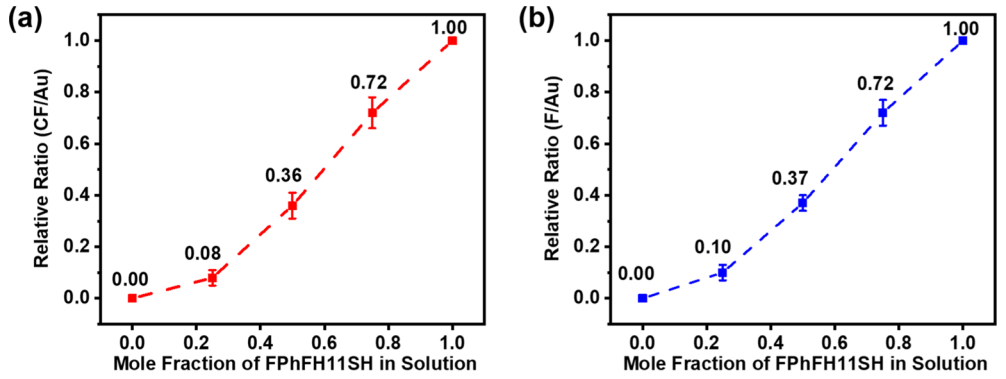

Figure 5. (a) CF/Au ratio and (b) F/Au ratio of the **PhH12SH/FPhFH11SH** mixed SAMs.

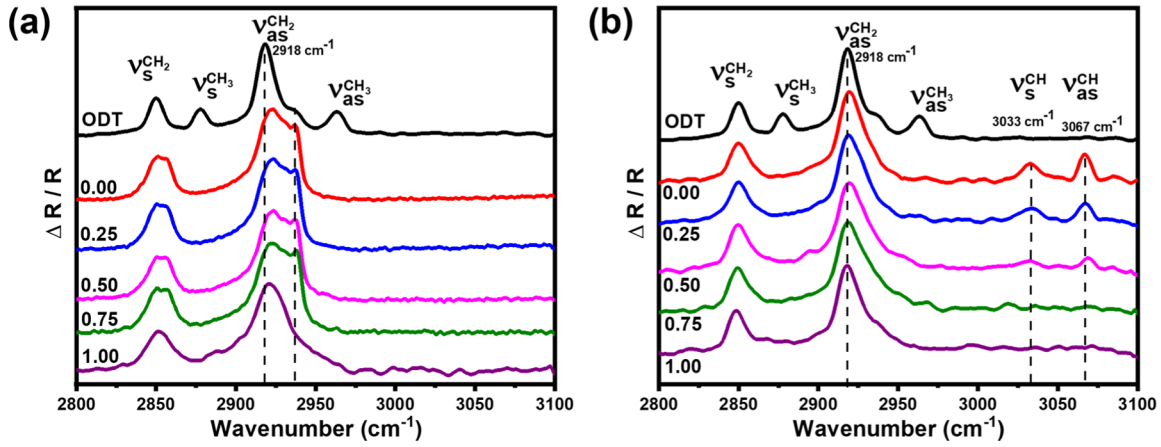

Figure 6. PM-IRRAS spectra of **ODT** and the mixed SAMs derived from (a) **HCyH11SH/FCyH11SH** and (b) **PhH12SH/FPhFH11SH**.

composition of the mixed SAMs; the CF from the aromatic ring at 288.3 eV was used in the analysis. The data in Figure 5a show the CF/Au ratios of **FPhFH11SH** (0.25), **FPhFH11SH** (0.50), and **FPhFH11SH** (0.75) at 0.08, 0.36, and 0.72, respectively. Following the same trend, the F/Au ratios in Figure 5b show **FPhFH11SH** (0.25), **FPhFH11SH** (0.50), and **FPhFH11SH** (0.75) having ratios of 0.10, 0.37, and 0.72, respectively. The ratios of the **FPhFH11SH** (0.25) and **FPhFH11SH** (0.50) SAMs indicate that the mole fraction of the **FPhFH11SH** adsorbate on the surface is lower than the mole fraction in solution with a slight preferential adsorption of the **PhH12SH** adsorbate, likely due to the difference in the steric bulk of the tail groups. However, in the case of the **FPhFH11SH** (0.75) SAM, the mole fraction of the adsorbate on the surface was the same as the mole fraction in solution, within an error. Regardless of the lower surface mole ratios of the former mixed SAMs, there is a linear trend in the data, suggesting that the **PhH12SH** and **FPhFH11SH** adsorbates adsorb onto the surface with similar tendencies.

The data suggest that there are two factors that may contribute to the observed phenomena: the solubility of the adsorbate in the deposition solution and molecular interactions between the tail groups. Previous studies show that in the case of the mixed SAMs derived from hexadecane-1-thiol and heptadecafluorohexadecane-1-thiol, poor solubility of the fluorinated adsorbate is the key factor that contributes to the preferential adsorption of it over its hydrocarbon analogue.[16−18] In the case of the **HCyH11SH/FCyH11H** mixed

https://doi.org/10.1021/acs.langmuir.2c01991
Langmuir 2022, 38, 13488−13496

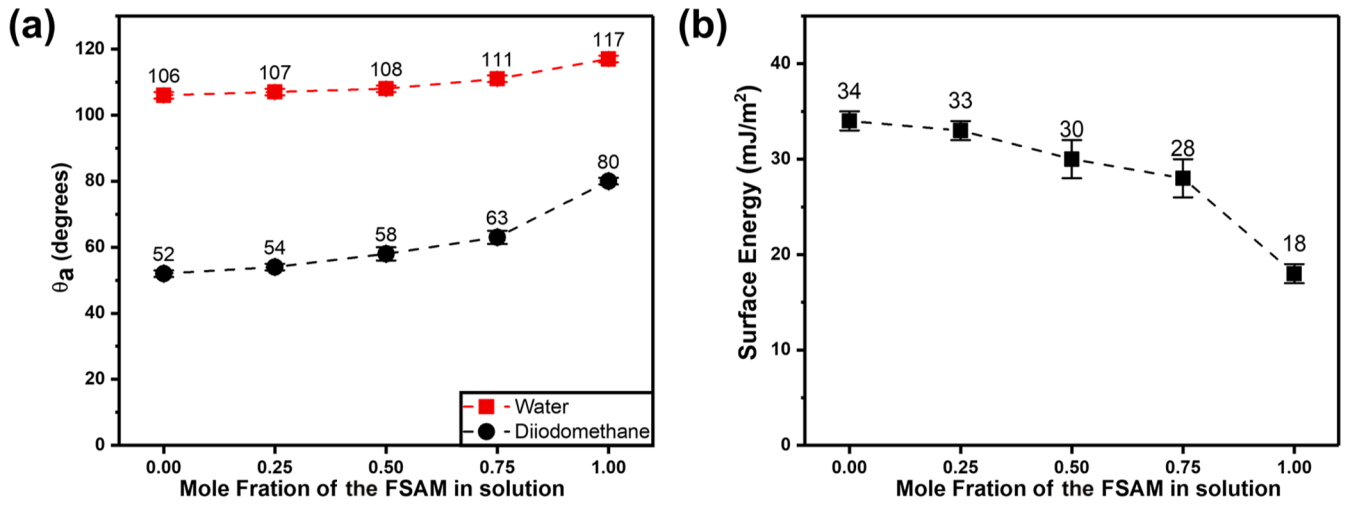

Figure 7. (a) Advancing contact angles of water and diiodomethane on the **HCyH11SH**/**FCyH11SH** mixed SAMs and (b) surface energies of the **HCyH11SH**/**FCyH11SH** mixed SAMs. Surface energies were calculated using the Owens−Wendt method.[47−50] Error bars are within the symbols.

SAMs, although it is also noticeable that **FCyH11SH** is harder to dissolve in ethanol than **HCyH11SH**, the steric bulkiness of the **FCyH11SH** adsorbate is likely a key factor that leads to significant preferential adsorption of the less bulky hydrocarbon adsorbate. The unfavorable dispersive interactions between the fluorocarbons and hydrocarbons in the tail groups of the adsorbates are likely an additional factor leading to the displacement of the fluorinated adsorbate from the surface. In the **PhH12SH**/**FPhFH11SH** mixed SAMs, the planar structure of the phenyl moieties coupled with $\pi-\pi$ interactions likely leads to a film that is closely representative to the deposition solution.[24,40] This is evidenced in the relatively higher packing densities than in the **HCyH11SH**/**FCyH11SH** mixed SAMs. The less bulky phenyl tail groups (compared to the bulkier cyclohexyl tail groups) and the interactions between the termini lead to homogeneously mixed SAMs derived from **PhH12SH** and **FPhFH11SH**. In addition, thanks to the special dielectric property of the π system, phenyl-terminated SAMs have been applied on field-effect transistors to tune the surface potentials and improve their performance.[41,42] The use of our mixed SAM films will allow researchers to control the surface composition of the SAMs in a systematic manner.

Assessment of Chain Conformational Order Using PM-IRRAS. PM-IRRAS is a surface infrared spectroscopy method that can be used to probe the relative chain conformational order of SAMs.[43] For well-ordered alkanethiol monolayers in which the hydrocarbon chains adapt all-trans extended crystalline conformations, such as the **ODT** SAM shown in Figure 6, the methylene antisymmetric stretching band ($\nu_{as}^{CH_2}$) is located at 2918 cm^{-1}.[44] On the other hand, disordered SAMs exhibit a blue shift in the $\nu_{as}^{CH_2}$ peak position.[45] Figure 6 shows the PM-IRRAS spectra of the **HCyH11SH**/**FCyH11SH** mixed SAMs and the **PhH12SH**/**FPhFH11SH** mixed SAMs in the C−H stretching region. All of the SAMs in the **HCyH11SH**/**FCyH11SH** series exhibit their $\nu_{as}^{CH_2}$ peak at 2851 ± 1 cm^{-1} with the single component SAMs in agreement with a previously published report.[2] We note that the broadening of the $\nu_{as}^{CH_2}$ and $\nu_{s}^{CH_2}$ peaks is due to an overlap between the peaks of the alkyl chain and the cyclohexane ring, which are observed in all of the spectra except for that of **FCyH11SH** (1.00).[2] For the **PhH12SH**/**FPhFH11SH** series, the $\nu_{as}^{CH_2}$ stretching band appeared at 2918 to 2919 cm^{-1}, which is consistent with the $\nu_{as}^{CH_2}$ position observed in a previous report.[30]

The PM-IRRAS spectra can also be used to obtain insights into the mixing of the adsorbates on the surface by monitoring peaks unique to one of the adsorbates. For the **HCyH11SH**/**FCyH11SH** series, the shoulder peak at 2937 cm^{-1}, which is unique to the cyclohexane ring, was used to monitor changes in the spectra. Conversely, for the **PhH12SH**/**FPhFH11SH** series, the peaks at 3033 and 3037 cm^{-1}, which arise from the phenyl ring, were used. Apparent from the data, all of the mixed SAMs in the **HCyH11SH**/**FCyH11SH** series, with the exception of **FCyH11SH** (1.00), exhibit C−H stretches from the cyclohexane ring, indicating that the surface is predominately composed of the **HCyH11SH** adsorbate, in accordance with the XPS data. In contrast, in the **PhH12SH**/**FPhFH11SH** series, there is a gradual decrease in the intensity of the aromatic C−H stretches in the spectra as the concentration of the fluorinated adsorbate is increased in the deposition solution. The gradual decrease observed in the spectra is indicative of a surface composed of both components, in agreement with the XPS data.

Contact Angle Measurements. The interfacial properties of the two mixed SAMs were characterized using contact angle measurements. The advancing contact angles (θ_a) of the mixed SAMs were measured using water (γ_{LV} = 72.0 mN/m) and diiodomethane (γ_{LV} = 50.0 mN/m) as the contacting liquids.[46] The surface energies of the mixed SAMs were also calculated using the Owens−Wendt method, which is commonly used in calculating the surface energies of organic thin films.[47−50] Figure 7 shows the advancing contact angles and surface energies of the mixed SAMs derived from the **HCyH11SH**/**FCyH11SH** series. Due to the hydrophobic and oleophobic nature of the fluorine atom, the FSAM, **FCyH11SH** (1.00), had higher water and diiodomethane contact angles, (117 and 80°, respectively) than its hydrocarbon analogue (106 and 52°, respectively), which is consistent with previous research.[2] The water and diiodomethane contact angles of the mixed SAMs remain relatively the same, with the exception of **FCyH11SH** (0.75) and **FCyH11SH** (1.00), where a significant increase in the contact angles are observed. We note that diiodomethane appears to be more sensitive than water toward the change of

https://doi.org/10.1021/acs.langmuir.2c01991
Langmuir 2022, 38, 13488−13496

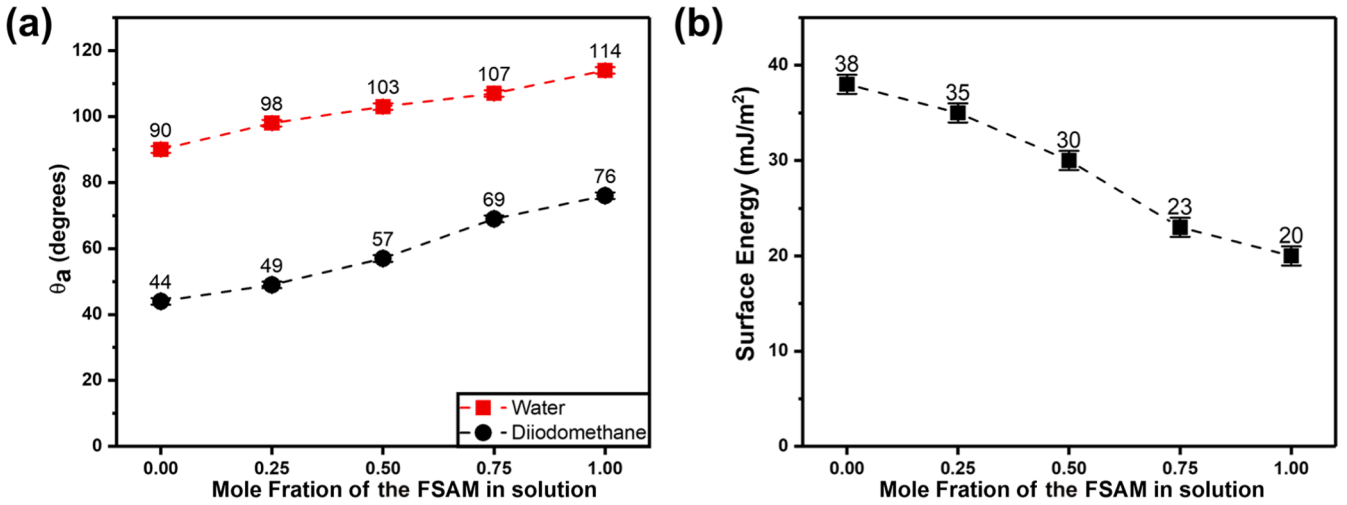

Figure 8. (a) Advancing contact angles of water and diiodomethane on the **PhH12SH**/**FPhFH11SH** mixed SAMs and (b) surface energies of the **PhH12SH**/**FPhFH11SH** mixed SAMs. Surface Energies were calculated using the Owens−Wendt method.[47−50] Error bars are within the symbols.

surface composition; this phenomenon can be attributed to the relatively large size of CH_2I_2 and the relatively large size of the fluorinated tail groups, which discourage penetration of this probe liquid into the films and limit the intermolecular interactions to the interfacial region. The surface energy of the mixed **HCyH11SH**/**FCyH11SH** SAM shows a consistent trend from 34 to 28 mJ/m^2, within error, on the **FCyH11SH** (0.00), **FCyH11SH** (0.25), **FCyH11SH** (0.75), and **FCyH11SH** (0.75) SAMs. However, from **FCyH11SH** (0.75) to **FCyH11SH** (1.00), surface energies dramatically change from 28 to 18 mJ/m^2. More importantly, the wettability and surface energies of the mixed SAMs derived from the **HCyH11SH**/**FCyH11SH** SAMs do not exhibit a linear relationship with the concentration of **FCyH11SH** in the deposition solution. These wettability behaviors limit the usage of this type of mixed SAMs to tune the wettability of surfaces. The contact angle data suggest that the interfacial properties of the SAMs resemble the hydrocarbon SAM, **HCyH11SH**, in agreement with the XPS and PM-IRRAS data.

Figure 8a shows the advancing contact angles and surface energies of the mixed SAMs derived from the **PhH12SH**/**FPhFH11SH** series. The water contact angle data of the single component SAMs, **FPhFH11SH** (0.00) and **FPhFH11SH** (1.00), indicates that the underlying CF_2−CH_2 (FC−HC) dipole does not affect the interfacial properties of the films. Previous reports with interfacial dipoles have seen lower water contact angles on these types of surfaces than in the analogous hydrocarbon SAM.[51] The perfluorophenyl tail group screens the FC−HC dipole, leading to a water contact angle that was higher than that of the phenyl-terminated SAM (114 vs 90°, respectively).[1] A similar trend is observed with the contact angle values of diiodomethane, 76° for the **FPhFH11SH** (1.00) SAM and 44° for the **FPhFH11SH** (0.00) SAM. Furthermore, the surface energies of the SAMs, shown in Figure 8b, exhibit a decreasing trend as the concentration of the fluorinated adsorbate is increased. More importantly, the contact angles of both test liquids and the surface energies exhibit a linear relationship with the composition of the solution, which is consistent with the XPS data. The data imply that the **PhH12SH**/**FPhFH11SH** SAMs can be used to tune the surface energy of the surface, ranging from 38 to 20 mJ/m^2.

CONCLUSIONS

In this study, two types of mixed SAMs derived from adsorbates terminated with either a cyclohexyl tail group (**HCyH11SH**) or a phenyl tail group (**PhH12SH**) mixed with their perfluorinated analogues (**FCyH11SH** and **FPhFH11SH**, respectively) were deposited on Au(111) surfaces. The XPS results show preferential adsorption of the nonfluorinated SAM in the **HCyH11SH**/**FCyH11SH** series. In the case of the **PhH12SH**/**FPhFH11SH** mixed SAMs, a linear relationship was observed between the mole fraction of the adsorbate on the surface and the mole fraction in solution. The relative solubility, steric bulk of the tail group moiety, and the interaction between two different adsorbates were determined to be major contributions to the preferential adsorption in the mixed SAMs of this class. Moreover, the mixed SAMs were also characterized using PM-IRRAS and contact angle goniometry measurements, and the surface energies of investigated surfaces were calculated using the Owens−Wendt method. In the case of the mixed SAMs derived from mixtures of **PhH12SH** and **FPhFH11SH**, the contact angles of the two test liquids and the surface energies show a linear relationship with respect to the mole fraction in solution, which was consistent with the composition determined from the XPS data. The results in this study suggest that the interfacial properties can be controlled with a minimal loss of packing densities with the **PhH12SH**/**FPhFH11SH** mixed SAMs on metal surfaces, which could prove useful in tuning the surface potential of organic thin-film transistors.

ASSOCIATED CONTENT

Supporting Information

The Supporting Information is available free of charge at https://pubs.acs.org/doi/10.1021/acs.langmuir.2c01991.

Materials and chemicals used, instrumental details, preparation of the Au substrates, the synthetic procedures and spectroscopic characterization data for the **FPhFH11SH** adsorbate (^{1}H, ^{19}F, and ^{13}C NMR spectra), and optical images of contact angles (PDF)

https://doi.org/10.1021/acs.langmuir.2c01991
Langmuir 2022, 38, 13488−13496

AUTHOR INFORMATION

Corresponding Author

T. Randall Lee − *Department of Chemistry and the Texas Center for Superconductivity and Department of Chemistry, University of Houston, Houston, Texas 77204-5003, United States;* orcid.org/0000-0001-9584-8861; Email: trlee@uh.edu

Authors

Tianlang Yu − *Department of Chemistry and the Texas Center for Superconductivity and Department of Chemistry, University of Houston, Houston, Texas 77204-5003, United States*

Maria D. Marquez − *Department of Chemistry and the Texas Center for Superconductivity and Department of Chemistry, University of Houston, Houston, Texas 77204-5003, United States*

Complete contact information is available at: https://pubs.acs.org/10.1021/acs.langmuir.2c01991

Notes

The authors declare no competing financial interest.

ACKNOWLEDGMENTS

We thank the National Science Foundation (CHE-2109174), the Robert A Welch Foundation (grant no. E-1320), and the Texas Center for Superconductivity at the University of Houston.

REFERENCES

(1) Zenasni, O.; Jamison, A. C.; Lee, T. R. The impact of fluorination on the structure and properties of self-assembled monolayer films. *Soft Matter* **2013**, *9*, 6356−6370.

(2) Yu, T.; Marquez, M. D.; Zenasni, O.; Lee, T. R. Mimicking Polymer Surfaces Using Cyclohexyl- and Perfluorocyclohexyl-Terminated Self-Assembled Monolayers. *ACS Appl. Nano Mater.* **2019**, *2*, 5809−5816.

(3) Kirchner, C.; George, M.; Stein, B.; Parak, W. J.; Gaub, H. E.; Seitz, M. Corrosion Protection and Long-Term Chemical Functionalization of Gallium Arsenide in an Aqueous Environment. *Adv. Funct. Mater.* **2002**, *12*, 266−276.

(4) Sharma, H.; Moumanis, K.; Dubowski, J. J. pH-Dependent Photocorrosion of GaAs/AlGaAs Quantum Well Microstructures. *J. Phys. Chem. C* **2016**, *120*, 26129−26137.

(5) Tkachev, M.; Anand-Kumar, T.; Bitler, A.; Guliamov, R.; Naaman, R. Enabling Long-Term Operation of GaAs-Based Sensors. *Engineering* **2013**, *05*, 1−12.

(6) Cui, M.; Wang, Y.; Wang, H.; Wu, Y.; Luo, X. A label-free electrochemical DNA biosensor for breast cancer marker BRCA1 based on self-assembled antifouling peptide monolayer. *Sens. Actuators, B* **2017**, *244*, 742−749.

(7) Taufik, S.; Barfidokht, A.; Alam, M. T.; Jiang, C.; Parker, S. G.; Gooding, J. J. An antifouling electrode based on electrode−organic layer−nanoparticle constructs: Electrodeposited organic layers versus self-assembled monolayers. *J. Electroanal. Chem.* **2016**, *779*, 229−235.

(8) Yapu, Z. Stiction and anti-stiction in MEMS and NEMS. *Acta Mech. Sin.* **2003**, *19*, 1−10.

(9) Maboudian, R.; Ashurst, W. R.; Carraro, C. Self-assembled monolayers as anti-stiction coatings for MEMS: characteristics and recent developments. *Sens. Actuators, A* **2000**, *82*, 219−223.

(10) Kasai, T.; Bhushan, B.; Kulik, G.; Barbieri, L.; Hoffmann, P. Micro/nanotribological study of perfluorosilane SAMs for antistiction and low wear. *J. Vac. Sci. Technol. B* **2005**, *23*, 995−1003.

(11) Marquez, M. D.; Zenasni, O.; Jamison, A. C.; Lee, T. R. Homogeneously Mixed Monolayers: Emergence of Compositionally Conflicted Interfaces. *Langmuir* **2017**, *33*, 8839−8855.

(12) Folkers, J. P.; Laibinis, P. E.; Whitesides, G. M. Self-assembled monolayers of alkanethiols on gold: comparisons of monolayers containing mixtures of short- and long-chain constituents with methyl and hydroxymethyl terminal groups. *Langmuir* **1992**, *8*, 1330−1341.

(13) Folkers, J. P.; Laibinis, P. E.; Whitesides, G. M.; Deutch, J. Phase behavior of two-component self-assembled monolayers of alkanethiolates on gold. *J. Phys. Chem.* **1994**, *98*, 563−571.

(14) Smith, R. K.; Reed, S. M.; Lewis, P. A.; Monnell, J. D.; Clegg, R. S.; Kelly, K. F.; Bumm, L. A.; Hutchison, J. E.; Weiss, P. S. Phase Separation within a Binary Self-Assembled Monolayer on Au{111} Driven by an Amide-Containing Alkanethiol. *J. Phys. Chem. B* **2001**, *105*, 1119−1122.

(15) Stranick, S. J.; Parikh, A. N.; Tao, Y. T.; Allara, D. L.; Weiss, P. S. Phase Separation of Mixed-Composition Self-Assembled Monolayers into Nanometer Scale Molecular Domains. *J. Phys. Chem.* **1994**, *98*, 7636−7646.

(16) Lee, H. J.; Jamison, A. C.; Lee, T. R. Two Are Better than One: Bidentate Adsorbates Offer Precise Control of Interfacial Composition and Properties. *Chem. Mater.* **2016**, *28*, 5356−5364.

(17) Kissa, E. *Fluorinated Surfactants and Repellents*, 2nd ed; Taylor & Francis, 2001.

(18) Banks, R. E.; Smart, B. E.; Tatlow, J. C. *Organofluorine Chemistry: Principles and Commercial Applications*; Springer, 1994.

(19) Arima, Y.; Iwata, H. Effect of wettability and surface functional groups on protein adsorption and cell adhesion using well-defined mixed self-assembled monolayers. *Biomaterials* **2007**, *28*, 3074−3082.

(20) Balamurugan, S.; Ista, L. K.; Yan, J.; López, G. P.; Fick, J.; Himmelhaus, M.; Grunze, M. Reversible protein adsorption and bioadhesion on monolayers terminated with mixtures of oligo(ethylene glycol) and methyl groups. *J. Am. Chem. Soc.* **2005**, *127*, 14548−14549.

(21) Gray, T. P.; Nishida, J.; Johnson, S. C.; Raschke, M. B. 2D Vibrational Exciton Nanoimaging of Domain Formation in Self-Assembled Monolayers. *Nano Lett.* **2021**, *21*, 5754−5759.

(22) Pikalov, A. A.; Yu, T.; Rodriguez, D.; Lee, H. J.; Lee, T. R.; Baldelli, S. Multicolor Chemical Imaging by Sum Frequency Generation Imaging Microscopy of Monolayers on Metal Surfaces. *J. Phys. Chem. C* **2020**, *124*, 16908−16917.

(23) Partes, C.; Sauter, E.; Gärtner, M.; Kind, M.; Asyuda, A.; Bolte, M.; Zharnikov, M.; Terfort, A. Reestablishing Odd−Even Effects in Anthracene-Derived Monolayers by Introduction of a Pseudo-C_{2v} Symmetry. *J. Phys. Chem. C* **2019**, *123*, 20362−20372.

(24) Azzam, W.; Subaihi, A. Influence of an alkyl spacer on the formation and structure of 4-Fluorobenzenethiol and 4-Fluorobenzenemethanethiol self-assembled monolayers on Au(111). *Surf. Interfaces* **2020**, *20*, 100544.

(25) Yoshioka, T.; Fujita, H.; Kimura, Y.; Hattori, Y.; Kitamura, M. Wide-range work function tuning in gold surfaces modified with fluorobenzenethiols toward application to organic thin-film transistors. *Flexible Printed* **2020**, *5*, 014011.

(26) Liu, J.; Kind, M.; Schüpbach, B.; Kafer, D.; Winkler, S.; Zhang, W.; Terfort, A.; Wöll, C. Triptycene-terminated thiolate and selenolate monolayers on Au(111). *Beilstein J. Nanotechnol.* **2017**, *8*, 892−905.

(27) Dichiarante, V.; Tirotta, I.; Catalano, L.; Terraneo, G.; Raffaini, G.; Chierotti, M. R.; Gobetto, R.; Baldelli Bombelli, F.; Metrangolo, P. Superfluorinated and NIR-luminescent gold nanoclusters. *Chem. Commun.* **2017**, *53*, 621−624.

(28) Fenwick, O.; Van Dyck, C.; Murugavel, K.; Cornil, D.; Reinders, F.; Haar, S.; Mayor, M.; Cornil, J.; Samorì, P. Modulating the charge injection in organic field-effect transistors: fluorinated oligophenyl self-assembled monolayers for high work function electrodes. *J. Mater. Chem. C* **2015**, *3*, 3007−3015.

(29) Hsu, S. M.; Lin, Y. C.; Chang, J. W.; Liu, Y. H.; Lin, H. C. Intramolecular interactions of a phenyl/perfluorophenyl pair in the formation of supramolecular nanofibers and hydrogels. *Angew. Chem., Int. Ed. Engl.* **2014**, *53*, 1921−1927.

(30) Lee, S.; Puck, A.; Graupe, M.; Colorado, R.; Shon, Y.-S.; Lee, T. R.; Perry, S. S. Structure, Wettability, and Frictional Properties of

Phenyl-Terminated Self-Assembled Monolayers on Gold. *Langmuir* **2001**, *17*, 7364−7370.
(31) Van Bondi, A. Der Waals Volumes and Radii. *J. Phys. Chem.* **1964**, *68*, 441−451.
(32) Vickerman, J. C.; Gilmore, I. S. *Surface Analysis− The Principal Techniques*, 2nd ed.; John Wiley & Sons: Chichester, 2009.
(33) Rittikulsittichai, S.; Park, C. S.; Jamison, A. C.; Rodriguez, D.; Zenasni, O.; Lee, T. R. Bidentate Aromatic Thiols on Gold: New Insight Regarding the Influence of Branching on the Structure, Packing, Wetting, and Stability of Self-Assembled Monolayers on Gold Surfaces. *Langmuir* **2017**, *33*, 4396−4406.
(34) Matthew, J. *Surface Analysis by Auger and X-ray Photoelectron Spectroscopy*; John Wiley & Sons, Ltd, 2004; Vol. *36*, pp 1647.
(35) Castner, D. G.; Hinds, K.; Grainger, D. W. X-ray photoelectron spectroscopy sulfur 2p study of organic thiol and disulfide binding interactions with gold surfaces. *Langmuir* **1996**, *12*, 5083−5086.
(36) Ishida, T.; Hara, M.; Kojima, I.; Tsuneda, S.; Nishida, N.; Sasabe, H.; Knoll, W. High Resolution X-ray Photoelectron Spectroscopy Measurements of Octadecanethiol Self-Assembled Monolayers on Au(111). *Langmuir* **1998**, *14*, 2092−2096.
(37) Park, J. S.; Vo, A. N.; Barriet, D.; Shon, Y. S.; Lee, T. R. Systematic Control of the Packing Density of Self-Assembled Monolayers Using Bidentate and Tridentate Chelating Alkanethiols. *Langmuir* **2005**, *21*, 2902−2911.
(38) Colorado, R.; Lee, T. R. Attenuation Lengths of Photoelectrons in Fluorocarbon Films. *J. Phys. Chem. B* **2003**, *107*, 10216−10220.
(39) Zenasni, O.; Marquez, M. D.; Jamison, A. C.; Lee, H. J.; Czader, A.; Lee, T. R. Inverted Surface Dipoles in Fluorinated Self-Assembled Monolayers. *Chem. Mater.* **2015**, *27*, 7433−7446.
(40) Mezour, M. A.; Voznyy, O.; Sargent, E. H.; Lennox, R. B.; Perepichka, D. F. Controlling C_{60} Organization through Dipole-Induced Band Alignment at Self-Assembled Monolayer Interfaces. *Chem. Mater.* **2016**, *28*, 8322−8329.
(41) Liu, Z.; Bol, A. A.; Haensch, W. Large-scale graphene transistors with enhanced performance and reliability based on interface engineering by phenylsilane self-assembled monolayers. *Nano Lett.* **2011**, *11*, 523−528.
(42) Chen, H.; Guo, X. Unique role of self-assembled monolayers in carbon nanomaterial-based field-effect transistors. *Small* **2013**, *9*, 1144−1159.
(43) Porter, M. D.; Bright, T. B.; Allara, D. L.; Chidsey, C. E. D. Spontaneously Organized Molecular Assemblies. 4. Structural Characterization of n-Alkyl Thiol Monolayers on Gold by Optical Ellipsometry, Infrared Spectroscopy, and Electrochemistry. *J. Am. Chem. Soc.* **1987**, *109*, 3559−3568.
(44) MacPhail, R. A.; Strauss, H. L.; Snyder, R. G.; Elliger, C. A. Carbon-Hydrogen Stretching Modes and the Structure of n-Alkyl Chains. 2. Long, All-Trans Chains. *J. Phys. Chem.* **1984**, *88*, 334−341.
(45) Snyder, R. G.; Strauss, H. L.; Elliger, C. A. Carbon-Hydrogen Stretching Modes and the Structure of n-Alkyl Chains. 1. Long, Disordered Chains. *J. Phys. Chem.* **1982**, *86*, 5145−5150.
(46) Smallwood, I. M. *Handbook of Organic Solvent Properties*; John Wiley & Sons: New York, 1996.
(47) Chinwangso, P.; Hill, L. R.; Marquez, M. D.; Lee, T. R. Unsymmetrical Spiroalkanedithiols Having Mixed Fluorinated and Alkyl Tailgroups of Varying Length: Film Structure and Interfacial Properties. *Molecules* **2018**, *23*, 2632−2653.
(48) Yang, Y.; Jamison, A. C.; Barriet, D.; Lee, T. R.; Ruths, M. Odd−Even Effects in the Friction of Self-Assembled Monolayers of Phenyl-Terminated Alkanethiols in Contacts of Different Adhesion Strengths. *J. Adhes. Sci. Technol.* **2010**, *24*, 2511−2529.
(49) Bai, J.; Cameron, J.; Wang, Q.; Yan, C.; Yao, C.; Chen, M.; Meng, H.; He, C.; Xu, X. Self-assembled monolayers induced performance difference in organic single crystal field-effect transistors. *Org. Electron.* **2019**, *75*, 105392−105398.
(50) Jung, M.-H.; Choi, H.-S. Characterization of octadecyltrichlorosilane self-assembled monolayers on silicon (100) surface. *Korean J. Chem. Eng.* **2010**, *26*, 1778−1784.
(51) Colorado, R.; Lee, T. R. Wettabilities of Self-Assembled Monolayers on Gold Generated from Progressively Fluorinated Alkanethiols. *Langmuir* **2003**, *19*, 3288−3296.

https://doi.org/10.1021/acs.langmuir.2c01991
Langmuir 2022, 38, 13488−13496